

# A Computationally Optimal Randomized Proper Orthogonal Decomposition Technique

Dan Yu, Suman Chakravorty

**Abstract**—In this paper, we consider the model reduction problem of large-scale systems, such as systems obtained through the discretization of partial differential equations. We propose a computationally optimal randomized proper orthogonal decomposition (RPOD\*) technique to obtain the reduced order model by perturbing the primal and adjoint system using Gaussian white noise. We show that the computations required by the RPOD\* algorithm is orders of magnitude cheaper when compared to the balanced proper orthogonal decomposition (BPOD) algorithm and BPOD output projection algorithm while the performance of the RPOD\* algorithm is much better than BPOD output projection algorithm. It is optimal in the sense that a minimal number of snapshots is needed. We also relate the RPOD\* algorithm to random projection algorithms. The method is tested on two advection-diffusion equations.

**Keywords**—*Model Reduction, Proper Orthogonal Decomposition (POD), Randomization Algorithm.*

## I. INTRODUCTION

In this paper, we are interested in the model reduction of large scale systems such as those governed by partial differential equations (PDE). The dimension of the system is large due to the discretization of the PDEs. For instance, consider the atmospheric dispersion of an air pollutant [1]. The emission of the contaminants on the ground level is shown in Fig. 1 with four point sources labeled from S1 to S4.

This is a three dimensional problem, and after discretizing the PDE, the dimension of the system is  $10^6$ . Therefore, we are interested in constructing a reduced order model (ROM) that can capture the input/output characteristics of the large model such that this ROM can then be used by a filtering algorithm for updating the states of the field, such as the Kalman filter. Also, the actuators and sensors could be placed anywhere in this field, which leads to a model reduction problem of a large-scale system with a large number of inputs/outputs. There are two popular contemporary model reduction techniques that have been studied in the past few decades: Principal component analysis (PCA) and randomization algorithms.

Among the PCA algorithms, Balanced Proper Orthogonal Decomposition (BPOD) [2], [3] based on the balanced truncation [4] and the snapshot Proper Orthogonal Decomposition (POD) technique [5] has been widely used. Balancing transformations are constructed using the impulse responses

D. Yu is with the Department of Aerospace Engineering, Texas A&M University, College Station, TX, 77840 USA e-mail: (yudan198811@hotmail.com).

S. Chakravorty is with the Department of Aerospace Engineering, Texas A&M University, College Station, TX 77840 USA e-mail: (schakrav@tamu.edu)

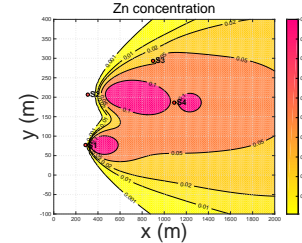


Fig. 1. Air pollutant problem

of both the primal and adjoint system, and hence, the most controllable and observable modes can be kept in the ROM. In 1978, Kung [6] presented a new model reduction algorithm in conjunction with the singular value decomposition (SVD) technique, and the eigensystem realization algorithm (ERA) [7] was developed based on this technique. The BPOD is equivalent to the ERA procedure [8], and forms the Hankel matrix using the primal and adjoint system simulations as opposed to the input-output data as in ERA. More recently, there has been work on obtaining information regarding the dominant modes of the system based on the snapshot POD, followed by an eigendecomposition of an approximating linear operator, called the dynamic mode decomposition (DMD) [9], [10]. In [11], [12], an adaptive POD algorithm based on the snapshot POD algorithm is introduced to recursively revise the locally valid ROMs. When there are new snapshots collected, decisions are made if the basis functions need to be updated. Both the DMD and adaptive POD algorithm are applicable for the nonlinear systems.

The primary drawback of the BPOD and ERA is that for a large scale system, such as that obtained by discretizing a PDE, with a large number of inputs/outputs, the computational burden incurred is very high. There are two main parts to the computation: the first is to collect datasets from computationally expensive primal and adjoint simulation in order to generate the Hankel matrix. The second part is to solve the SVD problem for the resulting Hankel matrix.

To reduce the computational cost of BPOD, improved algorithms have been proposed. For example, [3] proposed an output projection method to address the problem when the number of outputs is large. The outputs are projected onto a small subspace via an orthogonal projection  $P_s$  that minimizes the error between the full impulse response and the projected impulse response. However, the method cannot make any claim regarding the closeness of the solution to one that is obtained from the full Hankel matrix, and is still faced with a very high computational burden when both the numbers of inputs

and outputs are large. There have also been methods proposed [13] to reduce the number of snapshots, however, the primary problem regarding large number of inputs/outputs remains the same.

There are two major classes of randomization algorithms used for low-rank matrix approximations and factorizations: random sampling algorithms and random projection algorithms. For a large scale matrix  $H$ , random sampling algorithms construct a rank  $k$  approximation matrix  $\hat{H}$  by choosing and rescaling some columns of  $H$  according to certain sampling probabilities [14], so the error satisfies  $\|H - \hat{H}\|_F \leq \|H - H_{(k)}\|_F + \epsilon \|H\|_F$ , with high probability, where  $H_{(k)}$  is a best rank  $k$  approximation of  $H$ ,  $\epsilon$  is a specified tolerance, and  $\|H\|_F$  denotes the Frobenius norm of  $H$ . The improved algorithm proposed in [15] is to sample some columns according to leverage scores, where the leverage scores are calculated by performing the SVD of  $H$ , so that the error satisfies  $\|H - \hat{H}\|_F \leq (1 + \epsilon)\|H - H_{(k)}\|_F$ , with high probability. A direct application of both algorithms would require the full Hankel matrix to be constructed, however, such a construction of the Hankel matrix is computationally prohibitive when the number of inputs/outputs is large. Further, the leverage scores are calculated by performing the SVD of the Hankel matrix, which is also computationally prohibitive owing to the size of the problem.

In random projection method [16], the large matrix  $H$  is projected on to an orthonormal basis  $Q$  such that the error satisfies  $\|H - QQ'H\| \leq (1 + \epsilon)\|H - H_{(k)}\|$  with high probability, where  $\|H\|$  denotes the spectral 2-norm of  $H$ ,  $(\cdot)'$  denotes the conjugate transpose of  $(\cdot)$ . A Gaussian test matrix  $\Omega$  is generated, and the orthonormal basis  $Q$  is constructed by performing a QR factorization of the matrix product  $H\Omega$ . The bottleneck of this algorithm remains, as above, the construction of the full Hankel matrix, which is prohibitively expensive.

We had introduced an RPOD algorithm in [17] that randomly chooses a subset of the input/output trajectories. A sub-Hankel matrix is constructed using these sampled trajectories, which is then used to form a ROM in the usual BPOD fashion. The Markov parameters of the ROM constructed using the sub-Hankel matrix were shown to be close to the Markov parameters of the full order system with high probability. We proved that a lower bound exists for the number of the input/output trajectories that need to be sampled. The major problem associated with this algorithm is that different choices of the sampling algorithms would lead to different lower bounds, and the choice of a good sampling algorithm other than the uniform distribution is unclear.

In this paper, we propose the RPOD\* algorithm which is closely related to the random projection algorithm. In the RPOD\* algorithm, we perturb the primal and adjoint system with Gaussian white noise, and we prove that similar to the BPOD algorithm, the controllable and observable modes are retained in the ROM. The Markov parameters of the ROM constructed using RPOD\* are shown to be close to the Markov parameters of the full order system, while the error is bounded. The main contribution of the RPOD\* method is that it is computational orders of magnitudes less expensive when

compared to the BPOD/ERA and randomization algorithms for a large-scale system with a large number of inputs/outputs. The RPOD\* algorithm can be viewed as applying the random projection on the full Hankel matrix  $H$  twice without constructing the full Hankel matrix  $H$ , i.e.,  $\hat{H} = \Omega_2' Z' X \Omega_1 = \Omega_2' H \Omega_1$ , where  $\Omega_1, \Omega_2$  are two random projection matrices, and  $Z, X$  are the usual impulse response matrices of the adjoint and primal system. However, we actually only generate  $Z\Omega_2$  and  $X\Omega_1$  which can be constructed from a single white noise perturbed trajectory each of the adjoint and primal system respectively, and thus, are orders of magnitude smaller in size than the impulse responses  $Z$  and  $X$ . Thus, the computational cost to generate the Hankel matrix and to solve the SVD problem is saved by orders of magnitude. We believe that it is the most computational efficient POD algorithm. In practice, the RPOD\* algorithm can be solved in real-time.

The rest of the paper is organized as follows. In Section II, the problem is formulated, and in Section III, we review the BPOD algorithm and illustrate in a simplified fashion how to relate the BPOD ROM to the controllable and observable modes of the system. The RPOD\* algorithm is proposed in Section IV, and the formal proofs and results are shown. Also, we discuss some implementation problems in this section. In Section V, we compare the RPOD\* algorithm with BPOD output projection algorithm. In Section VI, we provide computational results comparing the RPOD\* with the BPOD/BPOD output projection for a one dimensional heat transfer problem and a three dimensional atmospheric dispersion problem.

## II. PROBLEM FORMULATION

Consider a stable linear input-output system:

$$\begin{aligned} x_k &= Ax_{k-1} + Bu_k, \\ y_k &= Cx_k, \end{aligned} \quad (1)$$

where  $x_k \in \mathbb{R}^N$ ,  $u_k \in \mathbb{R}^p$ ,  $y_k \in \mathbb{R}^q$  are the states, inputs, and outputs at discrete time instant  $t_k$  respectively. Assume that  $A, B, C$  matrices are real. The Markov parameters of the system is defined as  $CA^i B, i = 1, \dots$ .

The adjoint system is defined as:

$$z_k = A'z_{k-1} + C'v_k, w_k = B'z_k, \quad (2)$$

where  $z_k \in \mathbb{R}^N$ ,  $w_k \in \mathbb{R}^p$  is the state and output of the adjoint system at time  $t_k$  respectively,  $v_k \in \mathbb{R}^q$ .

Suppose  $A$  is diagonalizable, and let

$$A = V\Lambda U', \quad (3)$$

where  $\Lambda$  are the eigenvalues,  $(V, U)$  are the corresponding right and left eigenvectors.

A mode  $(\Lambda_i, U_i, V_i)$  is not controllable if  $U_i' B = 0$ , and is not observable if  $C V_i = 0$ , where  $(\Lambda_i, V_i, U_i)$  is the  $i^{th}$  eigenvalue-eigenvector pair.

Therefore, we partition the eigenvalues and eigenvectors

$(\Lambda, V, U)$  into four parts:

$$A = \begin{pmatrix} V'_{co} \\ V'_{c\bar{o}} \\ V'_{\bar{c}o} \\ V'_{\bar{c}\bar{o}} \end{pmatrix}' \begin{pmatrix} \Lambda_{co} & & & \\ & \Lambda_{c\bar{o}} & & \\ & & \Lambda_{\bar{c}o} & \\ & & & \Lambda_{\bar{c}\bar{o}} \end{pmatrix} \begin{pmatrix} U'_{co} \\ U'_{c\bar{o}} \\ U'_{\bar{c}o} \\ U'_{\bar{c}\bar{o}} \end{pmatrix}, \quad (4)$$

where  $(\Lambda_{co}, V_{co}, U_{co})$  are the controllable and observable modes,  $(\Lambda_{c\bar{o}}, V_{c\bar{o}}, U_{c\bar{o}})$  are the controllable but not observable modes,  $(\Lambda_{\bar{c}o}, V_{\bar{c}o}, U_{\bar{c}o})$  are the not controllable but observable modes, and  $(\Lambda_{\bar{c}\bar{o}}, V_{\bar{c}\bar{o}}, U_{\bar{c}\bar{o}})$  are the not controllable and not observable modes.

In this paper, we consider the model reduction problem for large-scale systems with a large number of inputs/outputs. The goal is to construct a ROM such that the outputs of the ROM  $y_r$  are close to the outputs of the full order system  $y$ , i.e.,  $|y - y_r|$  are bounded and all the controllable and observable modes of system  $(A, B, C)$  are preserved in the ROM.

### III. BALANCED PROPER ORTHOGONAL DECOMPOSITION

In this section, first, we briefly review the BPOD algorithm, and then give an informal proof to illustrate in a simplified fashion how the transformation bases and the Markov parameters of the ROM constructed using the BPOD algorithm can be related to the controllable and observable modes  $(\Lambda_{co}, V_{co}, U_{co})$  of the system matrix  $A$ . The simplified analysis is critical to understand the fundamentals of the proposed RPOD\* algorithm in Section IV.

#### A. BPOD Algorithm

The BPOD Algorithm [3] is briefly reviewed here. Consider the stable linear system (1)-(2), let  $B = [b_1, \dots, b_p]$  where  $b_i, i = 1, \dots, p$  is the  $i^{\text{th}}$  column of  $B$ , and  $C' = [c'_1, \dots, c'_q]$ , where  $c'_j, j = 1, \dots, q$  is the  $j^{\text{th}}$  row of  $C$ .

The impulse response of the primal system is collected using  $b_i, i = 1, \dots, p$  as the initial conditions for (1) with  $u_k = 0$ . We take  $m$  snapshots at discrete times  $t_1, t_2, \dots, t_m$ , and the primal snapshot ensemble  $X_b$  is:

$$X_b = [x_1(t_1), \dots, x_p(t_1), \dots, x_1(t_m), \dots, x_p(t_m)], \quad (5)$$

where  $x_i(t_k)$  is the state snapshot at time  $t_k$  with  $b_i$  as the initial condition,  $k = 1, 2, \dots, m$  and  $i = 1, 2, \dots, p$ .

Similarly, the adjoint snapshot ensemble is collected using  $c'_j, j = 1, \dots, q$  as initial conditions for (2) with  $v_k = 0$ . We take  $n$  snapshots at time step  $\hat{t}_1, \hat{t}_2, \dots, \hat{t}_n$ . The adjoint snapshot ensemble  $Z_b$  is:

$$Z_b = [z_1(\hat{t}_1), \dots, z_q(\hat{t}_1), \dots, z_1(\hat{t}_n), \dots, z_q(\hat{t}_n)], \quad (6)$$

where  $z_j(\hat{t}_k)$  is the state snapshot of the adjoint system at time  $\hat{t}_k$  with  $c'_j$  as the initial condition,  $k = 1, 2, \dots, n$  and  $j = 1, 2, \dots, q$ .

The Hankel matrix  $H_b$  is defined as

$$H_b = Z'_b X_b, \quad (7)$$

and we solve the SVD problem of  $H_b$ :

$$H_b = (L_b \quad L_1) \begin{pmatrix} \Sigma_b & 0 \\ 0 & 0 \end{pmatrix} \begin{pmatrix} R'_b \\ R'_1 \end{pmatrix}, \quad (8)$$

where  $\Sigma_b$  contains the first  $l$  non-zero singular values, and  $(L_b, R_b)$  are the corresponding left and right singular vectors. It is assumed that the rest of the singular values are approximately zero. The BPOD bases are:

$$T_b = X_b R_b \Sigma_b^{-1/2}, S_b = \Sigma_b^{-1/2} L'_b Z'_b, \quad (9)$$

and the ROM is:

$$A_b = S_b A T_b, B_b = S_b B, C_b = C T_b. \quad (10)$$

#### B. Simplified Analysis of BPOD

In the following, we provide a simplified analysis of the BPOD algorithm.

Consider the snapshots in the primal snapshot ensemble (5),

$$x_i(t_k) = A^{t_k-1} b_i, \quad (11)$$

where  $i = 1, \dots, p$  and  $k = 1, \dots, m$ . Hence,

$$(x_1(t_k), \dots, x_p(t_k)) = A^{t_k-1} B, \quad (12)$$

and the snapshot ensemble  $X_b$  can be written as:

$$X_b = (A^{t_1-1} B \quad A^{t_2-1} B \quad \dots \quad A^{t_m-1} B). \quad (13)$$

Assume  $A$  is diagonalizable, then from (4), we have:

$$\begin{aligned} A^{t_k-1} B &= (V_{co} \quad V_{c\bar{o}}) \begin{pmatrix} \Lambda_{co} & & \\ & \Lambda_{c\bar{o}} & \\ & & \end{pmatrix}^{t_k-1} \begin{pmatrix} U'_{co} \\ U'_{c\bar{o}} \end{pmatrix} B, \\ &= (V_{co} \quad V_{c\bar{o}}) \begin{pmatrix} \alpha_{co}^k \\ \alpha_{c\bar{o}}^k \end{pmatrix}, \end{aligned} \quad (14)$$

where  $U'_{\bar{c}o} B = 0, U'_{\bar{c}\bar{o}} B = 0$ , and  $\alpha_{co}^k, \alpha_{c\bar{o}}^k$  are the coefficient matrices. Thus,  $X_b$  can be written as:

$$X_b = (V_{co} \quad V_{c\bar{o}}) \begin{pmatrix} \alpha_{co}^b \\ \alpha_{c\bar{o}}^b \end{pmatrix}, \quad (15)$$

where  $\alpha_{co}^b, \alpha_{c\bar{o}}^b$  the coefficient matrices. Similarly,

$$Z_b = (U_{co} \quad U_{\bar{c}o}) \begin{pmatrix} \beta_{co}^b \\ \beta_{\bar{c}o}^b \end{pmatrix}, \quad (16)$$

where  $\beta_{co}^b, \beta_{\bar{c}o}^b$  are some coefficient matrices.

In the following, to simplify the analysis, let us assume that there are only controllable and observable eigenvectors present in the snapshot ensembles, i.e.,  $\alpha_{\bar{c}o}^b = 0, \beta_{\bar{c}o}^b = 0$ . Thus,

$$X_b = V_{co} \alpha_{co}^b, Z_b = U_{co} \beta_{co}^b. \quad (17)$$

Note that this assumption may not hold in practice, and is relaxed in the formal proof of our main result, Proposition 1, in Section IV.

Suppose there are  $l$  controllable and observable modes, then

$$Z'_b X_b = (\beta_{co}^b)' \alpha_{co}^b = L_b \Sigma_b R'_b, \quad (18)$$

where  $\Sigma_b \in \mathfrak{R}^{l \times l}$  are the  $l$  non-zero singular values and  $(L_b, R_b)$  are the corresponding left and right singular vectors. Moreover,

$$Z'_b A X_b = (\beta_{co}^b)' U'_{co} A V_{co} \alpha_{co}^b = (\beta_{co}^b)' \Lambda_{co} \alpha_{co}^b. \quad (19)$$

Now, consider the BPOD ROM:

$$\begin{aligned} A_b &= S_b A T_b = \Sigma_b^{-1/2} L'_b (Z'_b A X_b) R_b \Sigma_b^{-1/2} \\ &= \underbrace{\Sigma_b^{-1/2} L'_b (\beta_{co}^b)'}_{P_b} \Lambda_{co} \underbrace{\alpha_{co}^b R_b \Sigma_b^{-1/2}}_{\hat{P}_b}. \end{aligned} \quad (20)$$

We show that  $\Lambda_{co}$  are the eigenvalues of  $A_b$ , and  $P_b$  are the eigenvectors as follows:

$$\begin{aligned} P_b \hat{P}_b &= \Sigma_b^{-1/2} L'_b (\beta_{co}^b) \alpha_{co}^b R_b \Sigma_b^{-1/2} \\ &= \Sigma_b^{-1/2} L'_b L_b \Sigma_b R_b \Sigma_b^{-1/2} = I. \end{aligned} \quad (21)$$

Also,

$$\begin{aligned} \hat{P}_b P_b &= \alpha_{co}^b R_b \Sigma_b^{-1/2} \Sigma_b^{-1/2} L'_b (\beta_{co}^b)' \\ &= \alpha_{co}^b ((\beta_{co}^b)' \alpha_{co}^b)^+ (\beta_{co}^b)' = I, \end{aligned} \quad (22)$$

where  $(\cdot)^+$  denotes the pseudoinverse of  $(\cdot)$ . Hence,  $\hat{P}_b = P_b^{-1}$  and from (20),

$$\Lambda_{co} = \underbrace{(P_b^{-1} S_b)}_{\Phi_b} A \underbrace{(T_b P_b)}_{\Psi_b}. \quad (23)$$

Let  $(\Psi_b, \Phi_b)$  denote the new POD bases constructed by projecting  $(T_b, S_b)$  onto the ROM eigenspace, then

$$\begin{aligned} \Psi_b &= T_b P_b = X_b R_b \Sigma_b^{-1/2} \Sigma_b^{-1/2} L'_b (\beta_{co}^b)' \\ &= V_{co} \alpha_{co}^b R_b \Sigma_b^{-1} L'_b (\beta_{co}^b)' = V_{co} \hat{P}_b P_b = V_{co}, \end{aligned} \quad (24)$$

and similarly,

$$\Phi_b = P_b^{-1} S_b = U'_{co}, \quad (25)$$

i.e., under the approximation of exactly  $l$  controllable and observable modes being present in the snapshots, the modal coordinates of the BPOD ROM are precisely these  $l$  modes. Also, we prove that  $\Psi_b, \Phi_b$  are biorthogonal as follows.

$$\begin{aligned} \Psi_b \Phi_b &= T_b P_b P_b^{-1} S_b = T_b S_b, \\ \Phi_b \Psi_b &= P_b^{-1} S_b T_b P_b = P_b^{-1} P_b = I. \end{aligned} \quad (26)$$

Thus, the modal BPOD ROM constructed using  $(\Psi_b, \Phi_b)$  is:

$$\begin{aligned} \hat{A}_b &= \Phi_b A \Psi_b = \Lambda_{co}, \\ \hat{B}_b &= \Phi'_b B = U'_{co} B, \hat{C}_b = C \Psi_b = C V_{co}. \end{aligned} \quad (27)$$

*Remark 1:* From the analysis above, we see that the modal BPOD ROM consists of the controllable and observable modes, and is invariant to the data  $X_b$  and  $Z_b$ . Thus, we make the following observation.

As along as the snapshot ensembles are:

$$X = V_{co} \alpha, Z = U_{co} \beta, \quad (28)$$

where  $\alpha, \beta$  are some coefficient matrices, the modal ROM consists of the controllable and observable modes, and the ROM is given by (27).

*Remark 2:* Now, consider the impulse response snapshot

ensembles collected in the BPOD:

$$X_b = \underbrace{V_{co}}_{N \times l} \underbrace{\alpha_{co}^b}_{l \times pm}, Z_b = \underbrace{U_{co}}_{N \times l} \underbrace{\beta_{co}^b}_{l \times qn}, \quad (29)$$

and the Hankel matrix:

$$H_b = Z'_b X_b \in \mathbb{R}^{qn \times pm}. \quad (30)$$

There are two main parts to the computation:

- 1) The primal and adjoint snapshot ensembles  $X_b \in \mathbb{R}^{N \times pm}$ ,  $Z_b \in \mathbb{R}^{N \times qn}$ , and hence, the construction of  $H_b$  takes time  $O(pqmnN)$ .
- 2) The computational cost to solve the SVD of  $H_b$  is  $O(\min\{p^2 m^2 qn, pmq^2 n^2\})$ .

However, typically  $H_b$  is only rank " $l$ ", where  $l \ll N, pm, qn$ . Therefore, if we can generate optimal snapshot ensembles,

$$X^* = V_{co} \underbrace{\alpha^*}_{l \times l}, Z^* = U_{co} \underbrace{\beta^*}_{l \times l}, \quad (31)$$

where  $l \ll pm, qn$ ,  $\alpha^*, \beta^*$  are some coefficient matrices, then the BPOD result would still hold for the optimal snapshot ensembles  $X^*, Z^*$  while solving the SVD of  $H^* = (Z^*)' X^*$  would be reduced by orders of magnitude.

The snapshot ensembles  $X^*, Z^*$  are considered to be optimal because the rank of  $X^*, Z^*$  is  $l$ , and only  $l$  snapshots are needed to guarantee all the controllable and observable modes  $V_{co}, U_{co}$  would be preserved in  $X^*, Z^*$ .

Furthermore, given that only  $l$  snapshots are needed, the storage space of  $X^*, Z^*$  is also reduced by orders of magnitude from  $N \times qn, pm$  to  $N \times l$  since  $l \ll pm, qn$ . Bearing this observation in mind, in the next section, we introduce the RPOD\* algorithm which generates snapshot ensembles using white noise perturbations, such that (31) holds.

#### IV. COMPUTATIONALLY OPTIMAL RANDOMIZED PROPER ORTHOGONAL DECOMPOSITION (RPOD\*)

In this section, first, we give the reader the fundamental insight into the derivation of the RPOD\* algorithm. The RPOD\* algorithm is then formalized and treated rigorously in Section IV-B. We compare the RPOD\* algorithm with random projection in Section IV-C, we discuss implementation issues of the algorithm in Section IV-D.

##### A. Derivation of the RPOD\*

Consider the system (1)-(2), since  $A$  is stable, there exists a finite number  $t_{ss}$ , such that  $\|A^{t_{ss}}\| \approx 0$ . The primal snapshot ensemble collected in the BPOD are:  $X_b = (B \ AB \ \dots \ A^{t_{ss}-1} B) \in \mathbb{R}^{N \times pt_{ss}}$ . A Gaussian matrix  $\Omega_1 \in \mathbb{R}^{n \times m}$  is defined as:

$$\Omega_1 = \begin{pmatrix} \omega_{11} & \omega_{12} & \dots & \omega_{1m} \\ \vdots & \vdots & \dots & \vdots \\ \omega_{n1} & \omega_{n2} & \dots & \omega_{nm} \end{pmatrix}, \quad (32)$$

where each element  $\omega_{ij}$  of  $\Omega_1$  is an independent, identically distributed (i.i.d) variable with Gaussian distribution  $N(0, 1)$ .

Suppose  $m \leq n$ , in [16], it is shown that the columns of a Gaussian matrix  $\Omega_1$  are almost surely in general position, so  $\Omega_1$  has full column rank with probability one. Now we project the BPOD snapshot ensemble onto such a Gaussian matrix  $\Omega_1 \in \mathbb{R}^{pt_{ss} \times l}$ :

$$\underbrace{X^*}_{N \times l} = (X_1^* \quad X_2^* \quad \cdots \quad X_l^*) \\ = \underbrace{(B \quad \cdots \quad A^{t_{ss}-1}B)}_{X_b = V_{co} \alpha_{co}^b} \underbrace{\begin{pmatrix} \omega_{1,1} & \cdots & \omega_{1,l} \\ \vdots & \cdots & \vdots \\ \omega_{t_{ss},1} & \cdots & \omega_{t_{ss},l} \end{pmatrix}}_{\Omega_1}, \quad (33)$$

where  $\omega_{i,j} \in \mathbb{R}^{p \times 1}$ ,  $i = 1, \dots, t_{ss}$ ,  $j = 1, \dots, l$ . Suppose that the same assumption is made as in the heuristic analysis, i.e., only “1” controllable and observable modes are present in the snapshot ensemble  $X_b$ . The state snapshot  $X_j^*$  in  $X^*$  is:

$$X_j^* = \sum_{i=1}^{t_{ss}} A^{i-1} B \omega_{i,j}, \quad j = 1, \dots, l. \quad (34)$$

Since  $\Omega_1$  is a Gaussian matrix, each element of  $\Omega_1$  is an i.i.d Gaussian variable with distribution  $N(0, 1)$ , and thus,  $\omega_{i,j}$  is a Gaussian random vector with zero mean and covariance  $I_{p \times p}$ . Therefore,  $X_j^*$  is merely the snapshot of the primal system with a unit intensity white noise perturbation in each input channel, and given that  $\|A^{t_{ss}}\| \approx 0$ . Consequently,

$$X^* = V_{co} \alpha_{co}^b \Omega_1 = V_{co} \underbrace{\alpha^*}_{l \times l}, \quad (35)$$

and similarly, we may generate the adjoint snapshot ensembles  $Z^*$  by projecting  $Z_b$  onto the Gaussian matrix  $\Omega_2 \in \mathbb{R}^{qt_{ss} \times l}$ ,

$$Z^* = U_{co} \beta_{co}^b \Omega_2 = U_{co} \beta^*. \quad (36)$$

We know that  $X_b, Z_b$  are linear combinations of  $V_{co}, U_{co}$  respectively, thus, by projecting  $X_b, Z_b$  onto the Gaussian matrices, at least “ $l$ ” of the state snapshots in  $X^*, Z^*$  are still linearly independent, and  $X^*, Z^*$  are still linear combinations of  $V_{co}, U_{co}$ , since  $\Omega_1$  and  $\Omega_2$  are rank  $l$  with probability 1. Therefore, due to Remark 2, the SVD of  $H^* = (Z^*)' X^*$  would still result in obtaining the  $l$  controllable and observable modes while drastically reducing the computation in both computing the snapshots as well as the SVD.

From the analysis above, we see that the optimal snapshot ensembles (31) can be generated by collecting the white noise perturbation responses of system (1)-(2). We generate the snapshots as follows.

We perturb the primal system (1) with unit intensity white noise, i.e.,  $u_k \sim N(0, I)$ , and zero initial condition, then collect the snapshots at discrete time  $0 \leq t_1 < t_2 < \cdots < t_m$ , where  $t_m \geq t_{ss}$ , and  $\|A^{t_{ss}}\| \approx 0$ . The primal snapshot ensemble is:

$$X^* = [x(t_1), x(t_2), \dots, x(t_m)]. \quad (37)$$

The state response of primal system perturbed by the white

noise input  $u_k = u(t_k)$  at time  $t_k$  is:

$$x(t_k) = \sum_{i=0}^{t_k-1} A^{t_k-1-i} B u_i, \quad (38)$$

and the primal snapshot ensemble  $X^*$  can be written as:

$$X^* = X_b \underbrace{\begin{pmatrix} u(t_1-1) & \cdots & u(t_m-1) \\ u(t_1-2) & \cdots & u(t_m-2) \\ \vdots & \cdots & \vdots \\ 0 & \cdots & u(t_m-1-t_{ss}) \end{pmatrix}}_{\Omega_1}. \quad (39)$$

Thus, if we take the snapshots at time step  $t_1, \dots, t_m$ , since  $u_k \sim N(0, I)$  is white noise, then each column of  $\Omega_1$  is an i.i.d. Gaussian random vector, and the columns of  $\Omega_1$  are independent with probability 1 [16], and hence,  $\Omega_1$  has rank “ $l$ ” almost surely.

The adjoint snapshot ensemble  $Z^*$  is generated by collecting the white noise perturbation responses of the adjoint system through all the output channels in a similar fashion. The details regarding how to choose the snapshots are discussed in the subsection “Implementation Issues” at the end of this section.

In the following, the RPOD\* algorithm is proposed and the formal proof follows.

## B. RPOD\* Algorithm

The RPOD\* algorithm is summarized in Algorithm 1.

Given a stable linear system, the following result holds.

*Proposition 1:* Denote  $(A_r, B_r, C_r)$  as the ROM constructed using RPOD\* following Algorithm 1. Suppose there are  $l$  controllable and observable modes present in the snapshot ensembles  $X_r, Z_r$  collected using (40-41). Assume that the contribution of the not controllable modes in  $X_r$  and the contribution of the not observable modes in  $Z_r$  are relative small comparing to the other modes, i.e.,  $U'_{\bar{c}o} B = \epsilon C_1, U'_{\bar{c}o} B = \epsilon C_2, CV_{\bar{c}o} = \epsilon C_3, CV_{\bar{c}o} = \epsilon C_4$ , where  $C_1, C_2, C_3, C_4$  are some coefficient matrices, and  $\epsilon$  is a small number. If we keep the first  $l$  non-zero singular values, then  $\|C_r A_r^i B_r - C A^i B\| \propto O(\epsilon), i = 1, \dots$ .

*Proof:* The snapshot ensembles are expressed as follows, where all the eigenvectors are present in the snapshot ensembles, while we assume that the contribution of the not controllable modes in  $X_r$  and the contribution of the not observable modes in  $Z_r$  are relative small comparing to the other modes, i.e.,

$$U'_{\bar{c}o} B = \epsilon C_1, U'_{\bar{c}o} B = \epsilon C_2, CV_{\bar{c}o} = \epsilon C_3, CV_{\bar{c}o} = \epsilon C_4, \quad (47)$$

where  $C_1, C_2, C_3, C_4$  are some coefficient matrices, and  $\epsilon$  is a small number. Thus

$$X_r = V_{co} \alpha_{co} + V_{\bar{c}o} \alpha_{\bar{c}o} + V_{\bar{c}o} \delta \alpha_{\bar{c}o} + V_{\bar{c}o} \delta \alpha_{\bar{c}o}, \quad (48)$$

$$Z_r = U_{co} \beta_{co} + U_{\bar{c}o} \delta \beta_{\bar{c}o} + U_{\bar{c}o} \beta_{\bar{c}o} + U_{\bar{c}o} \delta \beta_{\bar{c}o}. \quad (49)$$

where  $\alpha_{co}, \alpha_{\bar{c}o}, \beta_{co}, \beta_{\bar{c}o}$  are the coefficient matrices, and

$$\delta \alpha_{\bar{c}o} = \left( \sum_{m=0}^{t_1-1} \Lambda_{\bar{c}o}^{t_1-1-m} U'_{\bar{c}o} B u_m, \sum_{m=0}^{t_2-1} \Lambda_{\bar{c}o}^{t_2-1-m} U'_{\bar{c}o} B u_m, \dots \right)$$

---

**Algorithm 1** RPOD\* Algorithm
 

---

- 1) Perturb the primal system (1) with white noise  $u_k$ , collect  $m$  snapshots at time step  $t_1, t_2, \dots, t_m$ , and denote the snapshot ensemble  $X_r$  as:

$$X_r = (x_1 \quad x_2 \quad \cdots \quad x_m). \quad (40)$$

- 2) Perturb the adjoint system (2) with white noise  $v_k$ , collect  $n$  snapshots at time step  $\hat{t}_1, \hat{t}_2, \dots, \hat{t}_n$ , and denote the adjoint snapshot ensemble  $Z_r$  as:

$$Z_r = (z_1 \quad z_2 \quad \cdots \quad z_n). \quad (41)$$

- 3) Solve the SVD problem:

$$Z_r' X_r = (L_r \quad L_o) \begin{pmatrix} \Sigma_r & 0 \\ 0 & \Sigma_o \end{pmatrix} \begin{pmatrix} R_r' \\ R_o' \end{pmatrix}, \quad (42)$$

and truncate at  $\sigma_l$ , where  $l$  is the number of controllable and observable modes present in the snapshot ensembles.  $\Sigma_r$  contains the first  $l$  non-zero singular values  $\sigma_1 \geq \sigma_2 \geq \dots \geq \sigma_l > 0$ ,  $(R_r, L_r)$  are the corresponding right and left singular vectors.

- 4) Construct the POD bases:

$$T_r = X_r R_r \Sigma_r^{-1/2}, S_r = \Sigma_r^{-1/2} L_r' Z_r'. \quad (43)$$

- 5) Construct the ROM  $\tilde{A}$ , find the eigenvalues  $\Lambda_r$  and eigenvectors  $P_r$  of  $\tilde{A}$ .

$$\tilde{A} = S_r A T_r = P_r \Lambda_r P_r^{-1}, \quad (44)$$

- 6) Construct new POD bases:

$$\Phi_r = P_r^{-1} S_r, \Psi_r = T_r P_r. \quad (45)$$

- 7) The ROM is:

$$A_r = \Phi_r A \Psi_r, B_r = \Phi_r B, C_r = C \Psi_r \quad (46)$$

$$= \epsilon \alpha_{\bar{c}o}, \quad (50)$$

and  $\alpha_{\bar{c}o}$  is a coefficient matrix. Similarly, we assume

$$\delta \alpha_{\bar{c}o} = \epsilon \alpha_{\bar{c}o}, \delta \beta_{\bar{c}o} = \epsilon \beta_{\bar{c}o}, \delta \beta_{\bar{c}o} = \epsilon \beta_{\bar{c}o}, \quad (51)$$

where  $\alpha_{\bar{c}o}, \beta_{\bar{c}o}, \beta_{\bar{c}o}$  are some coefficient matrices. Therefore,

$$\begin{aligned} Z_r' X_r &= \beta_{\bar{c}o}' \alpha_{\bar{c}o} + \delta \beta_{\bar{c}o}' \alpha_{\bar{c}o} + \beta_{\bar{c}o}' \delta \alpha_{\bar{c}o} + \delta \beta_{\bar{c}o}' \delta \alpha_{\bar{c}o} \\ &= \beta_{\bar{c}o}' \alpha_{\bar{c}o} + \epsilon \underbrace{(\beta_{\bar{c}o}' \alpha_{\bar{c}o} + \beta_{\bar{c}o}' \alpha_{\bar{c}o})}_{E_1} + O(\epsilon^2), \\ &= \beta_{\bar{c}o}' \alpha_{\bar{c}o} + \epsilon E_1 + O(\epsilon^2). \end{aligned} \quad (52)$$

And similarly,

$$\begin{aligned} Z_r' A X_r &= \beta_{\bar{c}o}' \Lambda_{\bar{c}o} \alpha_{\bar{c}o} + \epsilon \underbrace{(\beta_{\bar{c}o}' \Lambda_{\bar{c}o} \alpha_{\bar{c}o} + \beta_{\bar{c}o}' \Lambda_{\bar{c}o} \alpha_{\bar{c}o})}_{E_2} + O(\epsilon^2) \\ &= \beta_{\bar{c}o}' \Lambda_{\bar{c}o} \alpha_{\bar{c}o} + \epsilon E_2 + O(\epsilon^2). \end{aligned} \quad (53)$$

As we assumed before, there are “ $l$ ” controllable and observable modes, then  $\text{rank}(Z_r' X_r) \geq l$  due to the small

perturbations. Denote

$$\begin{aligned} \bar{H}_r &= \beta_{\bar{c}o}' \alpha_{\bar{c}o} = \bar{L}_r \bar{\Sigma}_r \bar{R}_r' + \bar{L}_o \bar{\Sigma}_o \bar{R}_o', \\ H_r &= Z_r' X_r = \beta_{\bar{c}o}' \alpha_{\bar{c}o} + \epsilon E_1 = L_r \Sigma_r R_r' + L_o \Sigma_o R_o, \end{aligned} \quad (54)$$

where  $\bar{H}_r, H_r \in \mathbb{R}^{n \times m}$ , and WLOG,  $n \leq m$ . Hence,  $\bar{H}_r$  is the ideal Hankel matrix constructed with the simplifying assumption that only controllable and observable modes present in the snapshot ensembles, and  $H_r$  is the true Hankel matrix which can be viewed as adding a small perturbation of  $\bar{H}_r$ .  $\bar{\Sigma}_r \in \mathbb{R}^{l \times l}$  contains the  $l$  non-zero singular values of  $\bar{H}_r$ , and  $(\bar{L}_r, \bar{R}_r)$  are the corresponding left and right singular vectors.  $\bar{\Sigma}_o \in \mathbb{R}^{(n-l) \times (n-l)} = 0$  are the rest singular values, and  $(\bar{L}_o, \bar{R}_o)$  are the corresponding left and right singular vectors. Similarly,  $\Sigma_r \in \mathbb{R}^{l \times l}$  contains the first  $k$  non-zero singular values of  $H_r$ , and  $\Sigma_o \in \mathbb{R}^{(n-l) \times (n-l)}$  contains the rest singular values. The left and right singular vectors are partitioned in the same way.

From the perturbation theory [18], for  $\bar{\sigma}_i \in \bar{\Sigma}_r$ , (strictly positive singular values) with multiplicity  $t$ ,  $\bar{L}_t, \bar{R}_t$  are the corresponding left and right singular vectors, the perturbed singular values  $\sigma_i \in \Sigma_r$ , and

$$\sigma_i = \bar{\sigma}_i + \epsilon \frac{\lambda_i(\bar{R}_t' E_1' \bar{L}_t + \bar{L}_t' E_1 \bar{R}_t)}{2} + O(\epsilon^2), i = 1, \dots, t \quad (55)$$

where  $\lambda_i(\cdot)$  denotes the  $i^{\text{th}}$  eigenvalue of  $(\cdot)$ . And the perturbed singular vectors [19]:

$$L_r = \bar{L}_r + \Delta L_r, R_r = \bar{R}_r + \Delta R_r, \quad (56)$$

where  $\Delta L_r, \Delta R_r$  are some matrices, and  $\|\Delta L_r\|, \|\Delta R_r\| \propto O(\epsilon)$ .

For  $\bar{\sigma}_i \in \bar{\Sigma}_o$  (zero singular values) [18] with multiplicity  $n - l$ , the corresponding left and right singular vectors are  $\bar{L}_o, \bar{R}_o$ . The perturbed singular values  $\sigma_i \in \Sigma_o$  and

$$\sigma_i = \epsilon \sqrt{\lambda_i(\bar{R}_o' E_1' \bar{L}_o \bar{L}_o' E_1 \bar{R}_o)}, i = 1, \dots, n - l. \quad (57)$$

The POD bases  $T_r, S_r$  are:

$$T_r = X_r R_r \Sigma_r^{-1/2}, S_r = \Sigma_r^{-1/2} L_r' Z_r'. \quad (58)$$

Therefore,

$$\begin{aligned} \tilde{A} &= \Sigma_r^{-1/2} L_r' Z_r' A X_r R_r \Sigma_r^{-1/2} \\ &= \Sigma_r^{-1/2} L_r' (\beta_{\bar{c}o}' \Lambda_{\bar{c}o} \alpha_{\bar{c}o} + \epsilon E_2) R_r \Sigma_r^{-1/2}. \end{aligned} \quad (59)$$

From (55), we have:

$$\Sigma_r = \begin{pmatrix} \sigma_1 & & \\ & \ddots & \\ & & \sigma_l \end{pmatrix} = \bar{\Sigma}_r + \begin{pmatrix} e_1 \epsilon & & \\ & \ddots & \\ & & e_l \epsilon \end{pmatrix}, \quad (60)$$

where  $e_1, \dots, e_l$  are the coefficients computed from (55). It can be proved that:

$$\Sigma_r^{-1/2} = \bar{\Sigma}_r^{-1/2} + \epsilon C_r, \quad (61)$$

where  $C_r$  is a diagonal coefficient matrix. Therefore,

$$\Sigma_r^{-1/2} L_r' = (\bar{\Sigma}_r^{-1/2} + \epsilon C_r) (\bar{L}_r' + \Delta L_r') = \bar{\Sigma}_r^{-1/2} \bar{L}_r' + \Delta_1, \quad (62)$$

where  $\Delta_1$  is some matrix, and  $\|\Delta_1\|_2 = k_1\epsilon$ ,  $k_1$  is a constant. Similarly,

$$R_r \Sigma_r^{-1/2} = \bar{R}_r \bar{\Sigma}_r^{-1/2} + \Delta_2, \quad (63)$$

where  $\Delta_2$  is some matrix, and  $\|\Delta_2\|_2 = k_2\epsilon$ ,  $k_2$  is a constant. Thus,

$$\tilde{A} = \underbrace{\bar{\Sigma}_r^{-1/2} \bar{L}'_r \beta'_{co}}_{\bar{P}_r} \Lambda_{co} \underbrace{\alpha_{co} \bar{R}_r \bar{\Sigma}_r^{-1/2}}_{\bar{P}_r^{-1}} + \Delta_3 + O(\epsilon^2), \quad (64)$$

where  $\Delta_3$  is some matrix, and  $\|\Delta_3\|_2 = k_3\epsilon$ ,  $k_3$  is a constant. As we have proved in Section III-B, if we let

$$\bar{A} = \bar{\Sigma}_r^{-1/2} \bar{L}'_r \beta'_{co} \Lambda_{co} \alpha_{co} \bar{R}_r \bar{\Sigma}_r^{-1/2}, \quad (65)$$

then  $\Lambda_{co}$  are the eigenvalues of  $\bar{A}$ , and  $\bar{P}_r$  are the corresponding eigenvectors. Since:

$$\tilde{A} = \bar{A} + \Delta_3 + O(\epsilon^2) = P_r \Lambda_r P_r^{-1}, \quad (66)$$

from the perturbation theory [20],  $\|P_r - \bar{P}_r\| \leq \|\Delta_3\| = k_3\epsilon$ ,  $\|\Lambda_r - \Lambda_{co}\| \leq \|\Delta_3\| = k_3\epsilon$ . Thus,

$$\begin{aligned} \Psi_r &= T_r P_r = X_r \bar{R}_r \bar{\Sigma}_r^{-1/2} \bar{P}_r + \Delta_4, \\ \Phi_r &= P_r^{-1} S_r = \bar{P}_r^{-1} \bar{\Sigma}_r^{-1/2} \bar{L}'_r Z'_r + \Delta_5, \end{aligned} \quad (67)$$

where  $\Delta_4, \Delta_5$  are some matrices and  $\|\Delta_4\|, \|\Delta_5\| \propto O(\epsilon)$ . Following the same proof in Section III-B, the ROM Markov parameters:

$$C_r A_r^i B_r = C \Psi_r \Lambda_r^i \Phi_r B = C V_{co} \Lambda_{co}^i U_{co} B' + \Delta, \quad (68)$$

where  $\Delta$  is some matrix, and  $\|\Delta\| \propto O(\epsilon)$ . ■

*Remark 3:* We assume that  $\epsilon$  is a small number, and we prove that  $\epsilon$  can also be related to  $\sigma_{l+1}$  as follows.

From (55) and (57), we can see that:

$$\sigma_l = \bar{\sigma}_l + e_l \epsilon + O(\epsilon^2), \sigma_{l+1} = e_{l+1} \epsilon, \quad (69)$$

Hence, we have:

$$\sigma_{l+1} \propto O(\epsilon), \quad (70)$$

and

$$\|C_r A_r^i B_r - C A^i B\| \propto O(\epsilon) \propto O(\sigma_{l+1}). \quad (71)$$

### C. Relation to the Random Projection

From the analysis in Section IV-A, we see that the snapshot ensembles collected in RPOD\* can be written as:

$$X_r = X_b \Omega_1, Z_r = Z_b \Omega_2, \quad (72)$$

where  $X_b \in \mathbb{R}^{N \times p t_{ss}}$ ,  $Z_b \in \mathbb{R}^{N \times q t_{ss}}$  are the impulse response snapshot ensembles that need to be collected in the BPOD algorithm from time step  $(1, \dots, t_{ss})$ , and  $\|A^{t_{ss}}\| \approx 0$ .  $\Omega_1 \in \mathbb{R}^{p t_{ss} \times m}$  and  $\Omega_2 \in \mathbb{R}^{q t_{ss} \times n}$  are Gaussian random matrices. We have:

$$\underbrace{H_r}_{\text{rank } l} = Z'_r X_r = \Omega'_2 Z'_b X_b \Omega_1 = \Omega'_2 \underbrace{H_b}_{\text{rank } l} \Omega_1, \quad (73)$$

There is a significant difference between the proposed algorithm and a direct application of the random projection

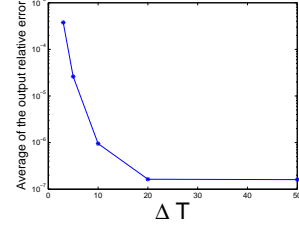


Fig. 2. Snapshot Selection: Effect of  $\Delta T$

algorithm on BPOD. A direct application of the random projection would require to generate the Hankel matrix  $H_b$  (and  $X_b, Z_b$ ) first. However, in practice, the construction and the storage of the Hankel matrix is computationally prohibitive when  $N$  is large and the number of inputs/outputs is large. Also, the bottleneck of the random projection algorithm is the projection of  $X_b, Z_b$  onto the Gaussian test matrices. In the proposed algorithm, the snapshot ensembles are constructed directly from the primal and adjoint simulations, and hence, the computational cost to generate the Hankel matrix and to project it onto the Gaussian test matrices is saved.

### D. Implementation Issues

Here we discuss some implementation problems in the RPOD\* algorithm. We give the insight into how to collect the snapshot ensembles, and how to select the ROM size.

**Snapshot selection** From the analysis in Section IV-B, we only need to collect  $m = l_1$  snapshots from the primal simulations, where  $l_1$  is the number of the controllable modes. However,  $l_1$  is not known a priori, thus, in practice, we start with a random guess  $m \ll N$ , where  $N$  is the dimension of the system, or we can choose  $m$  from experience. For instance, in a fluid system with  $10^6$  degrees of freedom,  $m$  is  $O(10) \sim O(10^2)$ . Similarly, we guess  $n$ , and then we check the rank of  $Z'_r X_r$ . If  $Z'_r X_r$  has full rank, i.e.,  $\text{rank}(Z'_r X_r) = \min(m, n)$ , then it is possible that we did not take enough snapshots, and hence, we increase  $m, n$ , until  $\text{rank}(Z'_r X_r) < \min(m, n)$ .

For the primal simulation, we take  $m$  snapshots from one simulation with zero initial condition, and white noise perturbation  $u(k)$ . We assume that the snapshots are taken at  $\Delta T, 2\Delta T, \dots, m\Delta T$ , WLOG. Here,  $\Delta T$  is a small constant, and we require that  $m\Delta T \geq t_{ss}$ , where  $\|A^{t_{ss}}\| \approx 0$ . In Fig. 2, we show one simulation result comparing the accuracy of the ROMs using  $\Delta T = 3, 5, 10, 20, 50$  for the atmospheric dispersion problem introduced in Section VI-B. Here  $t_{ss} = 900$ , and  $m = 300$ . The output relative error is defined in (80), and we take the average of the output relative error for each ROM. It can be seen that as  $\Delta T$  increases, each column in  $\Omega_1$  is well separated, and hence, the ROM is more accurate, while it takes longer time to generate the snapshots. Thus, this is a trade-off between the accuracy and the computational efficiency.

**ROM size selection** In Proposition 1, we assume that there are  $l$  controllable and observable modes, and we keep exact  $l$  non-zero singular values. However,  $l$  is not known a priori.

It is shown in Appendix A that if we keep  $k$  non-zero singular values, and  $k > l$ , then undesired noise will be introduced. If  $k < l$ , not all the controllable and observable modes can be recovered. Therefore, in practice, we decide  $l$  by trial and error. Since  $\text{rank}(Z_r' X_r) \geq l$  is always true, we start with  $k = \text{rank}(Z_r' X_r)$ , and check the eigenvalues of  $\tilde{A} = SAT$ . From the development in Appendix A, we can see that when  $k > l$ ,  $k-l$  eigenvalues of  $\tilde{A}$  are small, which are the perturbations of the zero eigenvalues. If  $k \gg l$ , then the perturbations in the ROM is too large to be neglected, which results in unstable eigenvalues of  $\tilde{A}$ . Thus, we keep decreasing the value of  $k$  until  $\tilde{A}$  is stable. If there are some small eigenvalues which are approximately zero, from Appendix A, we know  $k > l$ , and we decrease the value of  $k$  until we reach a region  $[l, l+a]$ , where  $a$  is a small number, such that most of the eigenvalues of  $\tilde{A}$  remain the same for different value of  $k$  ( $l$  controllable and observable modes with  $k-l$  perturbations of the zero eigenvalues), then we stop and pick the number  $l$  as the number of non-zero eigenvalues of  $\tilde{A}$ .

## V. COMPARISON WITH BPOD OUTPUT PROJECTION

As we mentioned in Section III, when the number of the outputs  $q$  is large, the computation of the BPOD adjoint simulations may not be tractable. To reduce the number of the outputs, the output projection method in [3], [21] is proposed. In this section, we compare the RPOD\* algorithm with BPOD output projection algorithm. First, we briefly review the BPOD output projection method.

- 1) Collect the primal snapshot ensemble  $X_b$  in (5).
- 2) Compute the POD modes of the dataset  $Y_b = CX_b$ .

$$Y_b \phi_k = \lambda_k \phi_k, \lambda_1 \geq \dots \geq \lambda_n \geq 0, \quad (74)$$

where  $\lambda_k$  are the eigenvalues, and  $\phi_k$  are the corresponding eigenvectors. Thus, the POD modes  $\Theta_s = [\phi_1, \dots, \phi_s]$ , where  $s$  is the rank of the output projection, and  $s \ll q$ .

- 3) Collect the impulse responses of the adjoint system:

$$z_{k+1} = A' z_k + C' \Theta_s v, w = B' z_k. \quad (75)$$

The adjoint snapshot ensemble is denoted as  $Z_s$ .

- 4) Construct the Hankel matrix:

$$H_s = Z_s' X_b. \quad (76)$$

- 5) Solve the SVD problem of  $H_s$ , and construct the BPOD output projection bases as  $(T_s, S_s)$  using equations (8) and (9). The ROM is:

$$A_s = S_s A T_s, B_s = S_s B, C_s = \Theta_s' C T_s. \quad (77)$$

In the following, we compare the BPOD output projection method with RPOD\* algorithm. From (75), the adjoint snapshot ensemble  $Z_s$  can be written as:

$$\underbrace{Z_s}_{N \times st_{ss}} = (C' \Theta_s \quad A' C' \Theta_s \quad \dots \quad (A')^{t_{ss}} C' \Theta_s)$$

TABLE I. COMPUTATIONAL COMPLEXITY ANALYSIS FOR RPOD\* AND BPOD OUTPUT PROJECTION

| Construction of $H$ | RPOD*      | BPOD output projection |
|---------------------|------------|------------------------|
| Solve SVD           | $O(mnN)$   | $O(pst_{ss}^2 N)$      |
|                     | $O(m^2 n)$ | $O(p^2 st_{ss}^3)$     |

$$= \underbrace{(C' \quad A' C' \quad \dots \quad (A')^{t_{ss}} C')}_{Z_b} \underbrace{\begin{pmatrix} \Theta_s & & & \\ & \Theta_s & & \\ & & \dots & \\ & & & \Theta_s \end{pmatrix}}_{\Theta} \quad (78)$$

$$= \underbrace{Z_b}_{N \times qt_{ss}} \underbrace{\Theta}_{qt_{ss} \times st_{ss}}.$$

And hence, the projected Hankel matrix  $H_s$  is:

$$H_s = \Theta' Z_b' X_b = \Theta' H_b, \quad (79)$$

Recall that the adjoint snapshot ensembles collected in RPOD\* can be written as  $Z_r = Z_b \Omega_2$ , and the projected Hankel matrix in RPOD\* is  $H_r = \Omega_2' H_b \Omega_1$ . Thus, both the BPOD output projection and RPOD\* algorithms can be viewed as projecting the full order Hankel matrix onto a reduced order Hankel matrix with projection matrices  $\Theta$  and  $(\Omega_1, \Omega_2)$ . Now we discuss the differences between two algorithms.

First, the information preserved in  $H_s, H_r$  are not the same. The output projection  $P_s = \Theta_s \Theta_s'$  minimizes the 2-norm of the difference between the original transfer function and the output-projected transfer function, i.e.  $\|CA^i B - \Theta_s \Theta_s' CA^i B\|, i = 1, \dots$ , is minimized. Thus, the controllable and observable modes preserved in  $H_s$  are an approximation of those in  $H_b$ , while in RPOD\* algorithm, the exact controllable and observable modes are preserved using the Gaussian random projection matrix. As mentioned in [21], when  $s < l$ , where  $l$  is the number of non-zero Hankel singular values (number of controllable and observable modes), then only the first  $s$  Hankel singular values are the same as the full balanced truncations Hankel singular values.

Another difference between output projection algorithm and RPOD\* algorithm is that RPOD\* algorithm can be used when both the number of the inputs and outputs are large, while output projection can be used when the number of the inputs or the outputs is large. When the number of inputs is large, we can construct an input projection using the adjoint snapshot ensemble, but when both the number of inputs and outputs are large, the construction of the projection matrix is not helpful.

The comparison of the computational cost of the BPOD output projection algorithm with RPOD\* algorithm is shown in Table I. We collect  $m, n$  snapshots for RPOD\* algorithm respectively, and  $t_{ss}$  snapshots for BPOD output projection algorithm.  $N$  is the dimension of the system,  $p, q$  are the number of inputs and outputs respectively, the rank of the output projection is  $s$ , and without loss of generality, we assume  $p \leq q, m \leq n$ , and  $p \leq s$ .

Now we compare the computation time to generate the snapshot ensembles. If we denote  $T$  as the time to propagate the primal/adjoint system once, then for BPOD output projec-

tion algorithm,  $(p + s)$  simulations are needed, and for each simulation, we need to collect the snapshots up to  $t = t_{ss}$ . Thus, the total computation time to generate the snapshot ensembles is  $(p + s)t_{ss}T$ .

The RPOD\* algorithm needs 1 primal and 1 adjoint simulation till time  $m\Delta T, n\Delta T$  respectively, where  $m\Delta T \geq t_{ss}, n\Delta T \geq t_{ss}$ . When we choose  $\Delta T$  such that  $m\Delta T = t_{ss}, n\Delta T = t_{ss}$ , the performance of the ROM constructed using RPOD\* is better than those constructed using BPOD/BPOD output projection algorithm. While, the total computation time to generate the snapshot ensembles is  $2t_{ss}T$ , which means that RPOD\* computational cost is the same as BPOD in a single input single output (SISO) system. The comparison of the computation time to generate the snapshot ensembles is shown in Table III for two examples.

## VI. COMPUTATIONAL RESULTS

In this section, we show the comparison of RPOD\* with BPOD for two examples: a one-dimensional heat transfer problem, and a three dimensional atmospheric dispersion problem to illustrate the proposed algorithm.

First, we define the output relative error:

$$E_{output} = \frac{\|Y_{true} - Y_{rom}\|}{\|Y_{true}\|}, \quad (80)$$

where  $Y_{true}$  are the outputs of the full order system, and  $Y_{rom}$  are the outputs of the reduced order system.

The frequency response for multiple input multiple output systems can be represented by plotting the maximum singular value of the transfer function matrix  $\max(\sigma(H(j\omega)))$  as a function of frequency  $\omega$ . We define the frequency responses error as:

$$E_{fre}(j\omega) = |\max(\sigma(H_{true}(j\omega))) - \max(\sigma(H_{rom}(j\omega)))|, \quad (81)$$

where  $H_{true}(j\omega)$  is the transfer function of the full order system, and  $H_{rom}(j\omega)$  is the transfer function of the ROM.

### A. Heat Transfer

The equation for heat transfer by conduction along a slab is given by the partial differential equation:

$$\frac{\partial T}{\partial t} = \alpha \frac{\partial^2 T}{\partial x^2} + f, \quad (82)$$

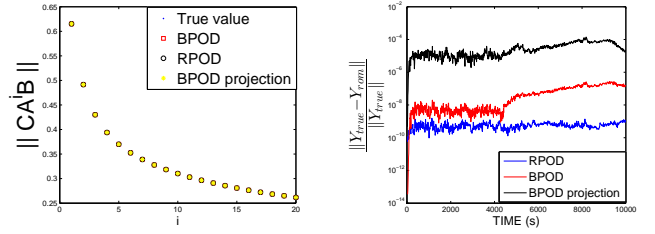
with boundary conditions

$$T|_{x=0} = 0, \quad \frac{\partial T}{\partial x}|_{x=L} = 0, \quad (83)$$

where  $\alpha$  is the thermal diffusivity, and  $f$  is the forcing.

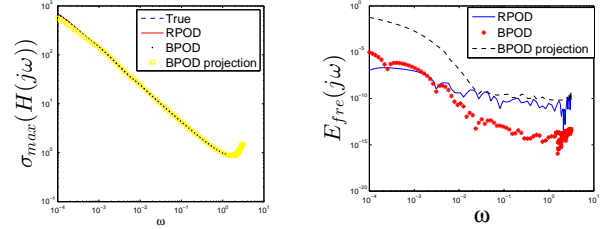
Two point sources are located at  $x = 0.15m$  and  $x = 0.45m$ . The system is discretized using finite difference method, and there are 100 grids which are equally spaced. We take full field measurements, i.e., measurements at every node. In the following, we compare the ROM constructed using RPOD\*, BPOD and BPOD output projection.

For RPOD\*, the system is perturbed by the white noise with distribution  $N(0, I_{2 \times 2})$ . At time  $t_{ss} = 3000s$ ,  $\|A^{t_{ss}}\| \approx 0$ ,



(a) Comparison of Markov Parameters (b) Comparison of Output Relative Errors

Fig. 3. Heat Transfer Problem



(a) Comparison of Frequency Responses (b) Comparison of Frequency Responses Errors

Fig. 4. Heat Transfer Problem

thus, for the primal/adjoint simulation, one realization is needed, and we collect 80 equispaced snapshots during time  $t \in [0, 3200]s$ . For BPOD, we need  $p = 2$  realizations for the primal simulation, and  $q = 100$  realizations for the adjoint simulations. In general, 3000 equispaced snapshots between  $[0, 3000]s$  should be taken in each realization for BPOD/output projection. However, due to the memory limits on the platform, only 400 equispaced snapshots can be taken and for the optimal performance of BPOD/output projection, the 400 equispaced snapshots are taken from time  $t \in [0, 400]s$  (first 400 dominant impulse responses). The rank of the output projection is 40, and hence, for the BPOD output projection algorithm, 40 realizations are needed for the adjoint simulations. RPOD\* algorithm and BPOD algorithm extract 70 modes, and BPOD output projection algorithm extract 50 modes. The parameters of the system are summarized in Table II. Here, we take 80 snapshots by trial and error following the procedure in Section IV-D.

In Fig. 3(a), we compare the norm of the Markov parameters of the ROM constructed using three algorithms with the true Markov parameters of the full order system. We perturb the system with random Gaussian noise, and compare the output relative errors in Fig. 3(b). In Fig. 4(a), we compare the frequency responses of the ROM constructed using three algorithms with the true frequency responses. In Fig. 4(b), we plot the error of the maximum singular value of the input-output model as a function of frequency.

For all three methods, we can see that the Markov parameters of the ROM are close to the true Markov parameters of the full order system. From Fig. 3(b), it can be seen that all three methods are accurate enough. The output relative

TABLE II. PARAMETERS OF SYSTEM

|                              |                        | Heat                                       | Atmospheric Dispersion                                       |
|------------------------------|------------------------|--|--|
| System Parameters            | Domain                 | $x \in [0, 1](m)$                          | $x \in [0, 2000](m), y \in [-100, 400](m), z \in [0, 50](m)$ |
|                              | Dimension of system    | $N = 100$                                  | $N = 10^5$   |
|                              | Parameters             | $\alpha = 4.2 \times 10^{-6}(m^2/s)$       | Wind velocity $\vec{u} = (4m/s, 0, 0)$                       |
|                              | Number of Inputs       | 2  | 10   |
|                              | Number of Outputs      | 100  | 810  |
| output projection V.S. RPOD* | Primal Snapshots       | 400 V.S. 80                                | 200 V.S. 400   |
|                              | Adjoint Snapshots      | 400 V.S. 80                                | 200 V.S. 400   |
|                              | Snapshots taken during | $t \in [0, 400s]$ V.S. $t \in [0s, 3200s]$ | $t \in [0, 200]s$ V.S. $t \in [0, 4000]s$                    |
|                              | ROM modes              | 50 V.S. 70                                 | 200 V.S. 380   |
|                              | Hankel matrix          | $16000 \times 800$ V.S. $80 \times 80$     | $4000 \times 2000$ V.S. $400 \times 400$                     |

error of BPOD output projection is less than 0.01%, and the performance of the RPOD\* algorithm is much better than the BPOD output projection algorithm, the performance of RPOD\* algorithm is better than BPOD algorithm because we do not take all the snapshots up to  $t_{ss}$  due to the memory limits. From Fig. 4, we can see that the frequency responses error of RPOD\* algorithm is smaller than BPOD and BPOD output projection algorithm in low frequencies. With the increase of the frequency, the BPOD algorithm performs better than RPOD\* algorithm, however, the errors are below  $10^{-10}$ , and hence, the difference is negligible. The comparison of computational time of RPOD\* and BPOD output projection algorithm is shown in Section VI-C. We can see that the construction of the snapshot ensembles using RPOD\* takes almost the same time as BPOD output projection, while the dominant computational cost is solving the SVD problem, and it can be seen that RPOD\* is about 24 times faster than BPOD output projection.

### B. Atmospheric Dispersion Problem

The three-dimensional advection-diffusion equation describing the contaminant transport in the atmosphere is:

$$\frac{\partial c}{\partial t} + \nabla \cdot (c\vec{u}) = \nabla \cdot (K(\vec{X})\nabla c) + Q\delta(\vec{X} - \vec{X}_s), \quad (84)$$

where

$c(\vec{X}, t)$ : mass concentration at location  $\vec{X} = (x, y, z)$ .

$\vec{X}_s = (x_s, y_s, z_s)$ : location of the point source.

$\vec{u} = (u\cos(\alpha), u\sin(\alpha), 0)$ : wind velocity.  $\alpha$  is the direction of the wind in the horizontal plane and the wind velocity is aligned with the positive  $x$ -axis when  $\alpha = 0$ ,  $u \geq 0$  is constant.

$Q$ : contaminant emitted rate.

$\nabla$ : gradient operator.

$K(\vec{X}) = \text{diag}(K_x(x), K_y(x), K_z(x))$ : diagonal matrix whose entries are the turbulent eddy diffusivities. In general  $K(\vec{X})$  is a function of the downwind distance  $x$  only.

In practice, the wind velocity is sufficiently large that the diffusion in the  $x$ -direction is much smaller than advection, and hence, assume that the term  $K_x \partial_x^2 c$  can be neglected.

Define  $\sigma_y^2(x) = \frac{2}{u} \int_0^x K_y(\eta) d\eta$ ,  $\sigma_z^2(x) = \frac{2}{u} \int_0^x K_z(\eta) d\eta$ , where  $\sigma_y(x) = a_y x(1 + b_y x)^{0.5}$ ,  $\sigma_z(x) = a_z x(1 + b_z x)^{0.5}$ , and  $a_y = 0.008$ ,  $b_y = 0.00001$ ,  $a_z = 0.006$ ,  $b_z = 0.00015$ .

The boundary conditions are:

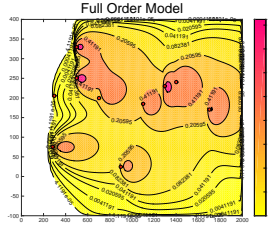
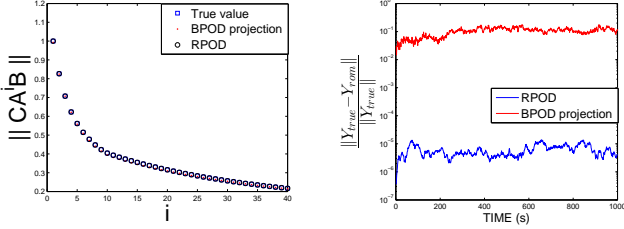
$$\begin{aligned} c(0, y, z) = 0, c(\infty, y, z) = 0, c(x, \pm\infty, z) = 0, \\ c(x, y, \infty) = 0, K_z \frac{\partial c}{\partial z}(x, y, 0) = 0. \end{aligned} \quad (85)$$

The system is discretized using finite difference method, and there are  $100 \times 100 \times 10$  grids which are equally spaced. The parameters are summarized in Table II. There are 10 point sources which are shown in Fig. 5. We take the full field measurements (except the nodes on  $x = 0, \infty$  and  $y = \pm\infty$ ). In Fig. 5, we show the actual concentration of the full field at time  $t = 200s$  with  $Q$  as Gaussian white noise where sources are the dotted points in the figure.

In this example, since the system dimension is  $N = 10^5$ , constructing the ROM with the full field measurements using BPOD is computationally impossible, and thus, we only compare the RPOD\* algorithm with BPOD output projection algorithm.

For RPOD\* algorithm, we collect the snapshots sequentially. The system is perturbed by white noise with distribution  $N(0, I_{10 \times 10})$ . One primal simulation and one adjoint simulation are needed. We collect 400 equispaced snapshots from time  $t \in [0, 4000]s$ , where at time  $t_{ss} = 4000$ ,  $\|A^{t_{ss}}\| \approx 0$ , and extract 380 modes. For BPOD output projection algorithm, we collect the impulse responses from the primal simulations, and  $p = 10$  realizations are needed. Same as the heat example, we could not collect all the impulse responses from  $t \in [0, 4000]s$  due to the memory limits on the platform. Hence, for the best performance available in this example, we collect 200 equispaced snapshots from  $t \in [0, 200]s$  for each primal simulation. The rank of the output projection is 80, and hence, 80 adjoint simulations are needed, and in the adjoint simulations, we collect 50 equispaced snapshots from  $t \in [0, 50]s$ . We can extract 200 modes. The parameters are summarized in Table II.

In Fig. 6(a), we compare the Markov parameters of the ROM constructed using RPOD\* and BPOD output projection with the full order system. Also, we perturb the system with random Gaussian noise, and compare the output relative errors in Fig. 6(b). The comparison of the computational time is shown in Section VI-C.

Fig. 5. Concentration Field at  $t = 200s$ 

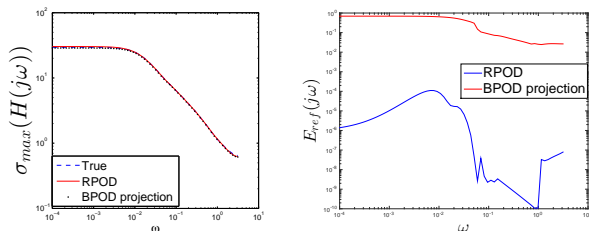
(a) Comparison of Markov Parameters (b) Comparison of Output Relative Errors

Fig. 6. Atmospheric Dispersion Problem

In Fig. 7(a), we compare the frequency responses of the ROM constructed using RPOD\* and BPOD output projection with the full order system. We can see that the frequency responses of the ROMs are almost the same as the frequency responses of the full order system. In Fig. 7(b), we show the errors between the frequency responses.

The comparison of the computational time is shown in Section VI-C. It can be seen that for this example, the construction of the snapshot ensembles using RPOD\* is faster than the BPOD output projection, and the dominant computation cost is the construction of  $Z^T X$ , where RPOD\* algorithm is almost 16500 times faster than BPOD output projection.

From the examples above, we can see that for both examples showed in this paper, the RPOD\* algorithm is much faster than BPOD/BPOD output projection algorithm, and is much more accurate than BPOD output projection algorithm.



(a) Comparison of Frequency Responses (b) Comparison of Frequency Responses Errors

Fig. 7. Atmospheric Dispersion Problem

### C. Comparison of Computational Time

Comparison of computational time is shown in Table III for two examples. All of the experiments reported in this paper were performed using Matlab 2013b on a Dell OptiPlex 9020, Intel(R) Core (TM) i7-4770CPU, 3.40GHz, 4GB RAM machine.

## VII. CONCLUSION

In this paper, we have introduced a computationally optimal randomized POD procedure for the extraction of ROMs for large scale systems such as those governed by PDEs. The ROM is constructed by perturbing the primal and adjoint system with Gaussian white noise, where the computational cost to construct the snapshot ensembles is saved when compared to perturbing the primal and adjoint system with impulses in BPOD/BPOD output projection algorithm. Also, it leads to a much smaller SVD problem, and an orders of magnitude reduction in the computation required for constructing ROMs over the BPOD/ BPOD output projection procedure. The computational results show that the accuracy of the RPOD\* is much more accurate than the BPOD output projection algorithm.

### APPENDIX

#### ROM SIZE SELECTION: $k > l$

Consider the SVD problem of  $H_r = Z_r^T X_r$ :

$$Z_r^T X_r = L \Sigma R, \quad (86)$$

where  $\Sigma = \text{diag}\{\sigma_1, \dots, \sigma_n\}$  is a diagonal matrix, and  $\sigma_1 \geq \sigma_2 \geq \dots \geq \sigma_n$  are the singular values,  $(R, L)$  are the right and left singular vectors. If we keep the first  $k$  singular values, and  $k \geq l$ , then denote

$$\Sigma_p = \begin{pmatrix} \sigma_1 & & & \\ & \ddots & & \\ & & \sigma_k & \\ & & & \end{pmatrix} = \begin{pmatrix} \Sigma_r & \\ & \Sigma_n \end{pmatrix}, \quad (87)$$

where  $\Sigma_r \in \mathbb{R}^{l \times l}$ ,  $\Sigma_n \in \mathbb{R}^{(k-l) \times (k-l)}$ . The corresponding left and right singular vectors can be partitioned in the same way, and are denoted as  $L_p = (L_r \ L_n)$ ,  $R_p = (R_r \ R_n)$ .

Then the transformation matrices are partitioned as:

$$S = \begin{pmatrix} S_1 \\ S_2 \end{pmatrix} = \begin{pmatrix} \Sigma_r^{-1/2} L_r^T Z_r^T \\ \Sigma_n^{-1/2} L_n^T Z_r^T \end{pmatrix}, \quad (88)$$

$$T = (T_1 \ T_2) = \begin{pmatrix} X_r R_r \Sigma_r^{-1/2} & X_r R_n \Sigma_n^{-1/2} \end{pmatrix}, \quad (89)$$

and thus,

$$\begin{aligned} \tilde{A} &= SAT = \begin{pmatrix} A_{11} & A_{12} \\ A_{21} & A_{22} \end{pmatrix} \\ &= \begin{pmatrix} \Sigma_r^{-1/2} L_r^T Z_r^T A X_r R_r \Sigma_r^{-1/2} & \Sigma_r^{-1/2} L_r^T Z_r^T A X_r R_n \Sigma_n^{-1/2} \\ \Sigma_n^{-1/2} L_n^T Z_r^T A X_r R_r \Sigma_r^{-1/2} & \Sigma_n^{-1/2} L_n^T Z_r^T A X_r R_n \Sigma_n^{-1/2} \end{pmatrix}. \end{aligned} \quad (90)$$

where from (66),  $A_{11} = P_r \Lambda_r P_r^{-1}$ , and as we proved in Proposition 1,  $\|P_r - \tilde{P}_r\| \propto O(\epsilon)$ ,  $\|\Lambda_r - \Lambda_{co}\| \propto O(\epsilon)$ .

TABLE III. COMPARISON OF COMPUTATIONAL TIME

|                 | Heat    |                               | Atmospheric Dispersion |                              |
|-----------------|---------|-------------------------------|------------------------|------------------------------|
|                 | RPOD*   | output projection             | RPOD*                  | output projection            |
| Generate $X$    | 0.0148s | 0.0518s                       | 55.59s                 | 30.461s                      |
| Generate $Z$    | 0.0340s | 0.0864s + 0.1582s(projection) | 56.23s                 | 421.99s + 9.287s(projection) |
| Construct $Z'X$ | 0.0292s | 0.0461s                       | 0.321s                 | 5311s                        |
| Solve SVD       | 0.1052s | 2.5550s                       | 0.4859s                | 9.118s                       |
| Total time      | 0.1832  | 2.8975s                       | 112.6269s              | 5781.856s                    |

Consider  $A_{12} \in \mathfrak{R}^{l \times (k-l)}$ .

$$A_{12} = \Sigma_r^{-1/2} L_r' Z_r' A X_r R_n \Sigma_n^{-1/2},$$

$$\|A_{12}\| \leq \|\Sigma_r^{-1/2} L_r' Z_r' A X_r R_n\| \|\Sigma_n^{-1/2}\|, \quad (91)$$

and  $\|\Sigma_n^{-1/2}\| = \sigma_k^{-1/2}$ , thus,

$$\|A_{12}\| \leq k_4 \sigma_k^{-1/2}, \|A_{21}\| \leq k_5 \sigma_k^{-1/2}, \|A_{22}\| \leq k_6 \sigma_k^{-1}. \quad (92)$$

where  $k_4, k_5, k_6$  are some constants. Therefore,

$$\tilde{A} = \begin{pmatrix} \bar{A}_{11} & 0 \\ 0 & 0 \end{pmatrix} + \underbrace{\begin{pmatrix} \Delta_3 & A_{12} \\ A_{21} & A_{22} \end{pmatrix}}_E \quad (93)$$

where

$$\|E\|^2 \leq \|E\|_F^2 = \|\Delta_3\|_F^2 + \|A_{12}\|_F^2 + \|A_{21}\|_F^2 + \|A_{22}\|_F^2$$

$$\leq l \|\Delta_3\|^2 + (k-l) \|A_{12}\|^2 + (k-l) \|A_{21}\|^2 + (k-l) \|A_{22}\|^2, \quad (94)$$

and suppose  $(k-l) \leq l$ . Hence,

$$\|E\| \leq k_3 \sqrt{l\epsilon} + k_7 \sqrt{k-l} \sigma_k^{-1/2} + k_6 \sqrt{k-l} \sigma_k^{-1}, \quad (95)$$

where  $k_7$  is a constant.

The eigenvalues of  $\begin{pmatrix} \bar{A}_{11} & 0 \\ 0 & 0 \end{pmatrix}$  are  $\bar{\Lambda}_{ij} = \begin{pmatrix} \Lambda_{co} & \\ & 0 \end{pmatrix}$ , and the corresponding eigenvectors are  $\bar{P}_{ij} = \begin{pmatrix} \bar{P} & 0 \\ 0 & I \end{pmatrix}$ , thus, the perturbed eigenvalues and eigenvectors of  $\tilde{A}$  are:

$$\tilde{A} = P_{ij} \Lambda_{ij} P_{ij}^{-1}, \quad (96)$$

where  $P_{ij} = \bar{P}_{ij} + \Delta_6$ ,  $\Lambda_{ij} = \bar{\Lambda}_{ij} + \Delta_7$ , and  $\Delta_6, \Delta_7$  are some matrices,  $\|\Delta_6\|, \|\Delta_7\| \propto O(\|E\|)$ . Thus,

$$\Psi = T P_{ij} = \begin{pmatrix} X_r \bar{R}_r \bar{\Sigma}_r^{-1/2} \bar{P} & 0 \\ & \Delta_8 \end{pmatrix},$$

$$\Phi = P_{ij}^{-1} S = \begin{pmatrix} \bar{P}^{-1} \bar{\Sigma}_r^{-1/2} \bar{L}_r' Z_r' & \\ & 0 \end{pmatrix} + \Delta_9, \quad (97)$$

and  $\Delta_8, \Delta_9$  are some matrices, and  $\|\Delta_8\|, \|\Delta_9\| \propto O(\|E\|)$ . Following the same proof in Section III-B, the ROM Markov parameters:

$$C_r A_r^i B_r = C \Psi \Lambda^i \Phi B = C V_{co} \Lambda_{co}^i U_{co}' B' + \Delta, \quad (98)$$

where  $\Delta$  is a matrix, and  $\|\Delta\| \propto O(\|E\|)$ . Thus, if we truncate at  $\sigma_k$ , and  $\sigma_k = O(\epsilon)$ , then  $\|E\| \propto O(\sigma_{k+1}^{-1})$ , and  $\|C_r A_r^i B_r - C A^i B\| \propto O(\sigma_k^{-1})$ . Therefore, the errors between the Markov parameters of the true system and the ROM system increase

as  $k$  increases, when  $k \geq l$ .

## REFERENCES

- [1] J. M. Stockie, "The mathematics of atmospheric dispersion modeling," *SIAM Review*, vol. 53, No.2, pp. 349–372, 2011.
- [2] K. Willcox and J. Peraire, "Balanced model reduction via the proper orthogonal decomposition," *AIAA Journal*, vol. 40, pp. 2323–2330, 2002.
- [3] C. W. Rowley, "Model reduction for fluids using balanced proper orthogonal decomposition," *International Journal of Bifurcation and Chaos*, vol. 15, pp. 997–1013, 2005.
- [4] B. C. Moore, "Principal component analysis in linear systems: Controllability, observability and model reduction," *IEEE Transactions on Automatic Control*, vol. 26, No.1, pp. 17–32, 1981.
- [5] G. Berkooz, P. Holmes, and J. L. Lumley, "The proper orthogonal decomposition in the analysis of turbulent flows," *Annual review of fluid mechanics*, vol. 25, pp. 539–575, 1993.
- [6] S. Kung, "A new identification method and model reduction algorithm via singular value decomposition," *12th Asilomar Conference on Circuits, Systems and Computers*, pp. 705–714, Nov. 1978.
- [7] J.-N. Juang and R. S. Pappa, "An eigensystem realization algorithm for model parameter identification and model reduction," *Journal of Guidance, Control, and Dynamics*, vol. 8, No.5, pp. 620–627, 1985.
- [8] Z. Ma, S. Ahuja, and C. W. Rowley, "Reduced order models for control of fluids using the eigensystem realization algorithm," *Theoret. Comput. Fluid Dyn.*, vol. 25, pp. 233–247, 2011.
- [9] P. J. Schmid, "Dynamic mode decomposition of numerical and experimental data," *Journal of Fluid Mechanics*, vol. 656, pp. 5–28, 2010.
- [10] J. H. Tu, C. W. Rowley, D. M. Luchtenburg, S. L. Brunton, and J. N. Kutz, "On dynamic mode decomposition: Theory and applications," *Journal of Computational Dynamics*, vol. 1, Issue 2, pp. 391–421, 2014.
- [11] D. B. Pourkargar and A. Armaou, "Geometric output tracking of nonlinear distributed parameter systems via adaptive model reduction," *Chemical Engineering Science*, vol. 116, pp. 418–427, 2014.
- [12] —, "Design of apod-based switching dynamic observers and output feedback control for a class of nonlinear distributed parameter systems," *Chemical Engineering Science*, vol. 136, pp. 62–75, 2015.
- [13] J. H. Tu and C. W. Rowley, "An improved algorithms for balanced pod through an analytic treatment of impulse response tails," *Journal of Computational Physics*, vol. 231, pp. 5317–5333, June, 2012.
- [14] P. Drineas *et al.*, "Fast monte carlo algorithms for matrices ii: Computing a low rank approximation to a matrix," *SIAM J. Computing*, vol. 36, pp. 158–183, 2006.
- [15] M. W. Mahnoey, "Randomized algorithms for matrices and data," arXiv: 1104.5557, Tech. Rep., 2011.
- [16] N. Halko, P. Martinsson, and J. Tropp, "Finding structure with randomness: probabilistic algorithms for constructing approximate matrix decompositions," *SIAM review*, vol. 52(2), pp. 217–288, 2011.
- [17] D. Yu and S. Chakravorty, "A randomized proper orthogonal decomposition technique," in *Proceedings of American Control Conference*, 2015, p. in press.

- [18] T. Soderstrom, "Perturbation results for singular values," Department of Information Technology at Uppsala University, Tech. Rep., 1999.
- [19] B. Friedlander and B. Porat, "First-order perturbation analysis of singular vectors in singular value decomposition," *IEEE Transactions on Signal Processing*, vol. 56, Issue 7, pp. 3044–3049, 2008.
- [20] T. Kato, *Perturbation Theory for Linear Operators*. New York: Springer-Verlag, 1995.
- [21] M. Ilak and C. W. Rowley, "Modeling of transitional channel flow using balanced proper orthogonal decomposition," *Physics of Fluids*, vol. 20, 2008.